Experimental verification of loss-induced field enhancement and collimation in anisotropic μ-near-zero metamaterials

Haitao Jiang,* Weiwei Liu, Kun Yu, Kai Fang, Yong Sun, Yunhui Li, and Hong Chen†
MOE Key Laboratory of Advanced Micro-Structured Materials, School of Physics Science and Engineering, Tongji University, Shanghai 200092, China
(Received 13 August 2014; revised manuscript received 24 November 2014; published 8 January 2015)

Intrinsic loss has long been thought to be a deteriorative factor in wave propagations. However, for metamaterials in which the real part of the permittivity or permeability vanishes, the role of loss is highlighted and can even lead to a topological transition of dispersion from a closed elliptic curve to an open hyperbolic curve. Based on two-dimensional transmission lines with lumped elements, anisotropic μ-near-zero metamaterials with engineered losses are realized. Loss-induced abnormal propagations including collimation and field enhancement governed by the topological transition are experimentally observed in transmission-line-based metamaterials.

DOI: 10.1103/PhysRevB.91.045302 PACS number(s): 78.67.Pt, 42.25.Bs, 78.20.Ci, 81.05.Xj

I. INTRODUCTION

Metamaterials with subwavelength units can realize various electromagnetic (EM) responses and provide new situations to revisit some fundamental phenomena in wave propagations. For example, negative refraction occurs when an EM wave enters a left-handed metamaterial [1]. How a wave propagates in a lossy material is also a basic problem. Intrinsic loss has long been thought to play a negative role in wave propagations. In a dielectric with a real index ($n_r > 1$) and intrinsic loss (α), if α increases, the transmission will decrease. However, if $n_r \ll \alpha$, for example, in zero-index metamaterials (ZIMs) with zero n_r and adjustable α, how will a wave propagate?

In ZIMs, the relative permittivity (ε) and/or permeability (μ) are zero. If only ε or only μ is near zero, the ZIM is also called an ε-near-zero (ENZ) or a μ-near-zero (MNZ) medium. In ZIMs, the phases of EM waves are the same everywhere [2] and the wavelength is greatly stretched [3]. As a result, ZIMs offer unprecedented ways to tailor the wave properties, including directive emission [4,5], light squeezing [6,7], scattering manipulation [8–12], etc. Moreover, previous perturbed parameters in dielectrics such as the nonlinear index, the magneto-optical component, and the loss are prominent now in the near-zero background index. So, in ZIMs the nonlinear effects [13,14] and rotation effects [15] are strongly enhanced. Recently, Feng theoretically found that the intrinsic loss in an ENZ medium can counterintuitively take a positive role in wave propagations and enhance transmissions [16]. Sun *et al.* used a silver-germanium stack to mimic an ENZ medium and numerically found the field enhancement and collimation by increasing the loss of the silver [17]. Although ENZ media have been realized by metal-dielectric stacks [18], owing to the difficulty of tuning metallic losses, this loss-induced phenomenon still needs to be observed in experiments. The experimental verifications of this phenomenon that can greatly expand the knowledge of wave propagations are highly desirable. In this paper, we use two-dimensional (2D) transmission lines (TLs) with lumped elements to realize loss-tunable MNZ media. Based on the topological transition of dispersion, we experimentally observe loss-induced field enhancement and collimation.

II. NEAR-ZERO PERMEABILITY REALIZED BY TRANSMISSION LINE

TLs with lumped elements can realize various EM parameters [19]. Our 2D TL fabricated on a FR-4 substrate with a thickness of $h = 1.6$ mm and relative permittivity of 4.75 is shown in Fig. 1. The width of the microstrip line is $w = 2.8$ mm. The structural factor of the TL is defined as $g = Z_0/\eta_{\text{eff}}$, where Z_0 and η_{eff} are the characteristic impedance and the effective wave impedance of the normal TL, respectively [20]. When $w > h$, $g = \frac{1}{w/h+1.393+0.667\ln(w/h+1.444)} = 0.255$. The sample contains a wedge part with a wedge angle of 15° and a rectangular part. The wedge part is a normal TL that is equivalent to a double-positive (DPS) medium with $\varepsilon = 7.1$ and $\mu = 1$ [20]. The rectangular part is a 8 (unit cell) × 9 (unit cell) TL in which series lumped capacitors (denoted by C) and resistors (denoted by R) are loaded in the y direction. The value of C is 2.5 pF in all samples. The unit sizes in the x direction and in the y direction (denoted by d) are 12 and 12.8 mm, respectively. The x and y components of the wave vectors are denoted by k_x and k_y, respectively. The transverse-electric polarization, i.e., the electric field in the z direction (E_z), is considered [21]. At first, only lumped capacitors are loaded. When the unit size is much smaller than the wavelength, the dispersion relation can be approximated as [21,22]

$$\frac{k_x^2}{\mu_y} + \frac{k_y^2}{\mu_x} = k_{\text{in}}^2, \tag{1}$$

where

$$\mu_x = 1 - \frac{1}{g\mu_0 C d(2\pi f)^2}, \tag{2}$$

$\mu_y = 1$, μ_0 is the permeability in vacuum, f is the frequency, and k_{in} is the wave vector in the normal TL. After the values of g, μ_0, C, and d are substituted into Eq. (2), the TL is described by an effective medium in which $\varepsilon = 7.1$, $\mu_y = 1$, and $\mu_x =$

*jiang-haitao@tongji.edu.cn
†hongchen@ tongji.edu.cn

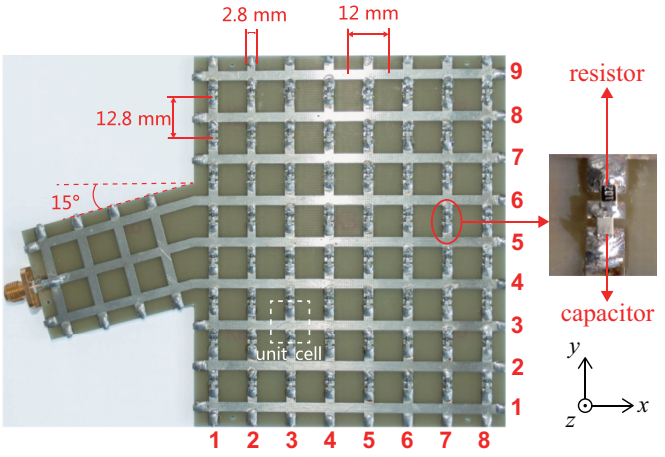

FIG. 1. (Color online) The sample contains a wedge part and a rectangular part. The wedge part is a normal TL. The rectangular part is a 8×9 TL in which series lumped capacitors and resistors are loaded in the y direction. The unit size in the rectangular part is 12 (mm) $\times$ 12.8 (mm). Insets show the amplified capacitor and resistor, respectively.

$1 - \beta^2/(2\pi f)^2$, where $\beta = 10.199$ GHz. Some isofrequency curves (IFCs) of this 2D medium are shown in Fig. 2. Here, $f = 1.623$ GHz, corresponding to $\mu_x = 0$, is a transition point. Below 1.623 GHz, $\mu_x < 0$, the IFCs are hyperbolic curves (see the curve at $f = 1.104$ GHz). Above 1.623 GHz, $\mu_x > 0$, the IFCs are elliptic curves, and near 1.623 GHz, the IFC is a very flat elliptic curve (see the curves at $f = 1.935$ and 1.639 GHz, respectively).

Equation (2) is an approximate model for the TL at the subwavelength unit cell condition. There would be a minor discrepancy between the model and the realistic TL. To obtain

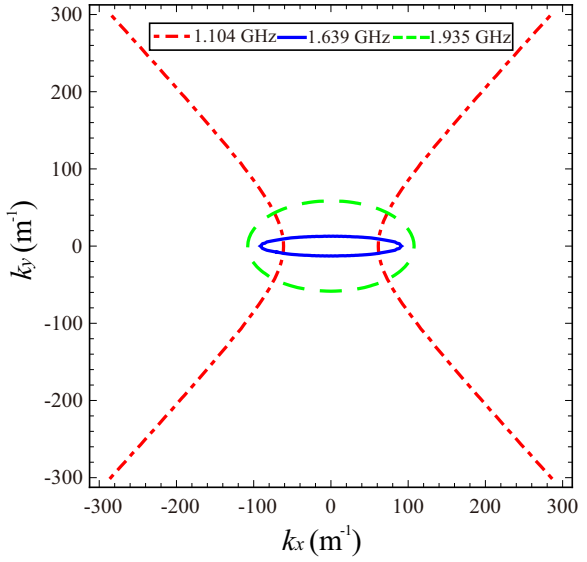

FIG. 2. (Color online) Some IFCs of a 2D medium in which $\varepsilon = 7.1$, $\mu_y = 1$, and $\mu_x = 1 - \beta^2/(2\pi f)^2$, where $\beta = 10.199$ GHz. Here, $f = 1.623$ GHz corresponding to $\mu_x = 0$ is a transition point. From $f < 1.623$ GHz to $f > 1.623$ GHz, the IFCs change from hyperbolic curves to elliptic curves.

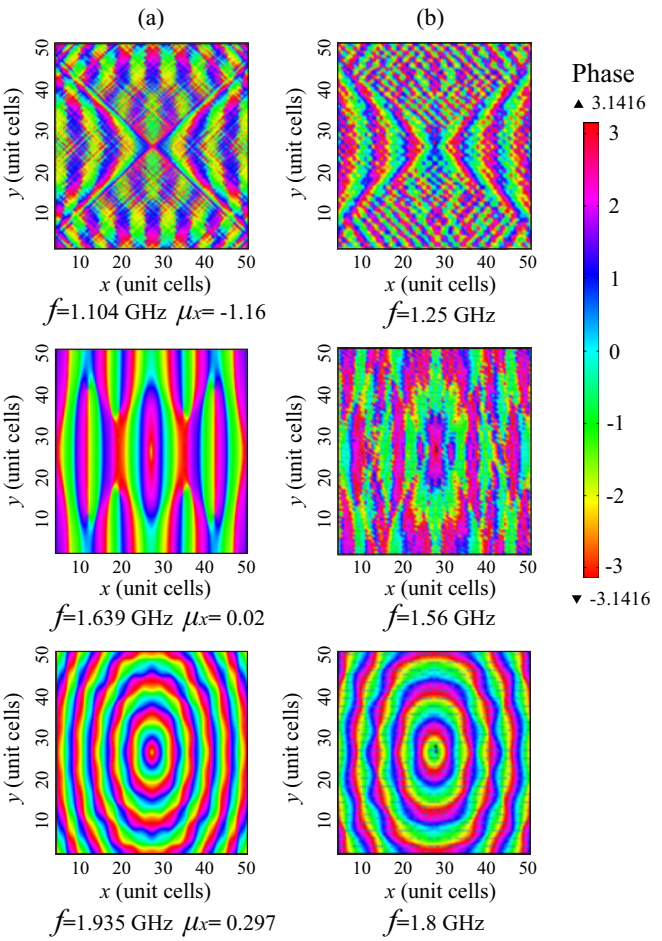

FIG. 3. (Color online) The phase distributions of E_z when a current source is put at the center of (a) the 2D medium described by the model and (b) the 51×51 TL that is the amplifying version of the TL with lumped capacitors in Fig. 1. The side lengths in the two cases are the same.

an accurate value of μ_x at the transition point in a realistic TL, we use computer simulation technology (CST) microwave studio software based on a finite integration method to simulate two square samples with the same sizes. One sample is a 2D medium with $\varepsilon = 7.1$, $\mu_y = 1$, and μ_x given by Eq. (2). At the sample edge, an open boundary condition is used. The other sample is a realistic 51 (unit cell) $\times$ 51 (unit cell) TL in which resistors with $R = 50\ \Omega$ are loaded at the edge to absorb waves. The same current source with an amplitude of 1 A is put at the center of each sample. The 51×51 TL is merely the amplifying version of the TL with lumped capacitors in Fig. 1. The phase distributions of E_z in each sample are given by Figs. 3(a) and 3(b), respectively. We test the frequency band from 1 to 2 GHz with a very small frequency step and find that, for a similar phase pattern, the frequency deviates a little for the model and the TL. For example, the phase patterns in Fig. 3(a) when $f = 1.104$, 1.639, and 1.935 GHz are very similar to those in Fig. 3(b) when $f = 1.25$, 1.56, and 1.8 GHz, respectively. The phase patterns can be explained by the IFCs in Fig. 2. After calculating many phase patterns in the TL near 1.56 GHz, we find that $f = 1.56$ GHz corresponds to a transition point at which the phase is most similar to that of a

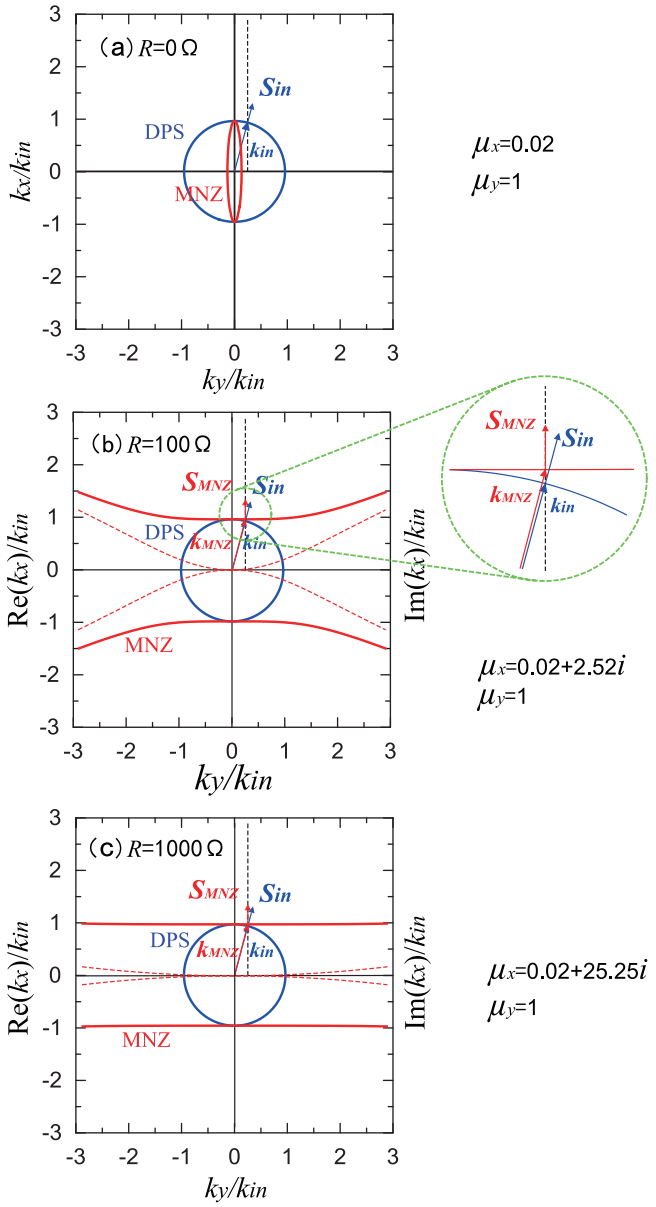

FIG. 4. (Color online) IFCs of the MNZ medium with a tunable loss (the red curves) and the DPS medium (the blue curves) at 1.639 GHz. In (a)–(c), $R = 0$, 100, and 1000 Ω, respectively. The incident (refracted) wave vector and the Poynting vector in DPS (MNZ) medium are denoted by k_{in} (k_{MNZ}) and S_{in} (S_{MNZ}), respectively. The angle of incidence is 15°. k_{in} and S_{in} are amplified in the inset.

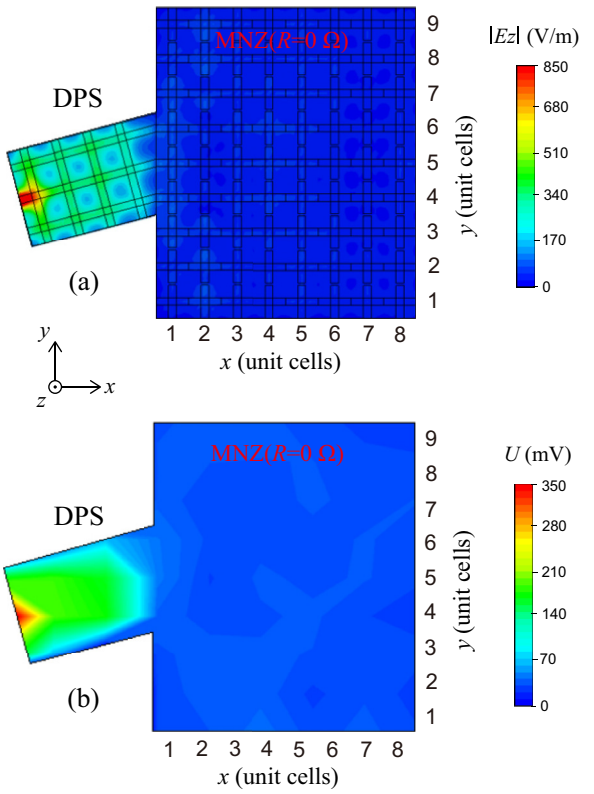

FIG. 5. (Color online) (a) The simulated $|E_z|$ pattern near the surface of the sample without lumped resistors ($R = 0$ Ω) and (b) the measured voltage amplitude (U) pattern in the sample at 1.56 GHz.

wave but only with a k_x component. From Eq. (2), $\mu_x = 0.02$ at 1.639 GHz. Therefore, we can only obtain the transition point corresponding to $\mu_x = 0.02$ rather than $\mu_x = 0$ in the TL at 1.56 GHz.

Now we load the lumped resistors in the TL to introduce intrinsic losses. The lumped capacitors, together with the resistors, can be seen as a compound capacitor with

$$C' = \frac{C}{1 + R^2\omega^2C^2} + \frac{R\omega C^2}{1 + R^2\omega^2C^2}i. \tag{3}$$

Replacing C in Eq. (2) with C', we obtain the complex μ_x. It should be pointed out that the imaginary part of μ_x could be large and only the real part of μ_x maintains near zero. In this case, when we refer to the MNZ material, we specifically refer to the near-zero real part of the permeability. When $R =$ 100 and 1000 Ω, at $f = 1.639$ GHz, $\mu_x = 0.02 + 2.52i$ and $0.02 + 25.16i$, respectively. Substituting the complex μ_x into Eq. (1), in Figs. 4(a)–4(c) we show the IFCs when $R = 0$, 100, and 1000 Ω, respectively. The IFCs give the relation between the real (imaginary) part of k_x and k_y [see the red solid (dotted) lines]. The closed elliptic curve in Fig. 4(a) changes to an open hyperbolic curve in Fig. 4(b) after loss is introduced. Note that this change is a topological transition [23]. In a normal dielectric, the loss as a perturbed parameter cannot change the topological property of dispersion. However, in a MNZ medium, the role of loss is highlighted and can even lead to a topological transition that strongly modifies the wave propagations. Moreover, when loss increases, the hyperbolic curve becomes flat and the imaginary part of k_x decreases. In Fig. 4 the IFCs of the DPS medium are plotted with blue curves. The incident (refracted) wave vector and the Poynting vector in DPS (MNZ) medium are denoted by k_{in} (k_{MNZ}) and S_{in} (S_{MNZ}), respectively. The angle of incidence is 15°. In Fig. 4(a), the k_y at an angle of 15° cannot be conserved in two media and total reflection occurs. However, in Figs. 4(b) and 4(c), as loss increases, the wave can go and collimate in the MNZ medium.

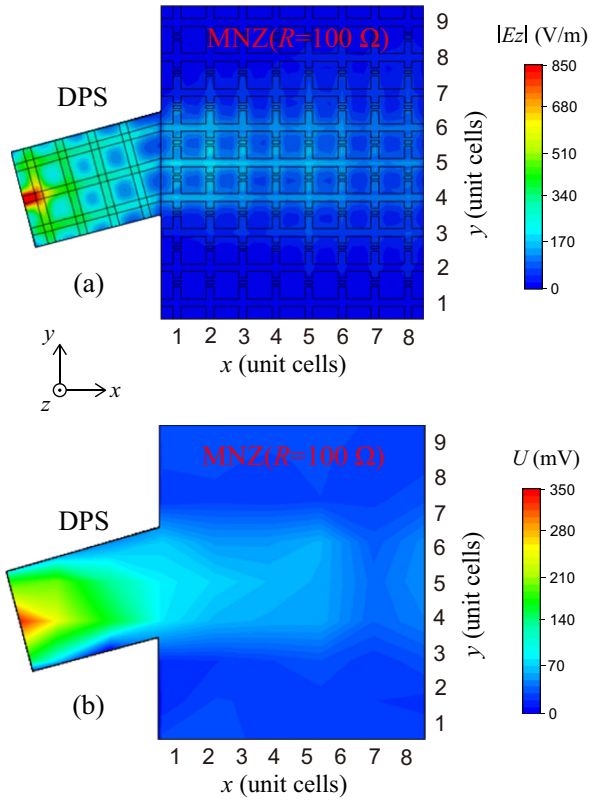

FIG. 6. (Color online) (a) The simulated $|E_z|$ pattern near the surface of the sample with $R = 100\ \Omega$ and (b) the measured U pattern in the sample at 1.56 GHz.

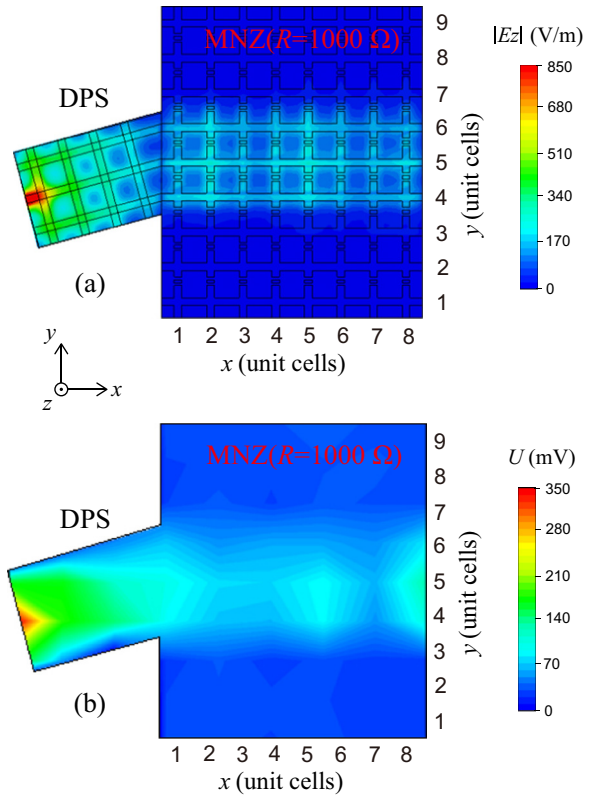

FIG. 7. (Color online) (a) The simulated $|E_z|$ pattern near the surface of the sample with $R = 1000\ \Omega$ and (b) the measured U pattern in the sample at 1.56 GHz.

III. EXPERIMENTAL VERIFICATION OF LOSS-ENHANCED TRANSMISSION

Here we use three samples with $R = 0$, 100, and 1000 Ω, respectively, as is shown in Fig. 1, to perform the experiments. At each sample edge, resistors with $R = 50\ \Omega$ are loaded to absorb waves. In simulations and experiments, we use voltage sources and the amplitudes between the metallic line and the ground plane for all sources are kept at 1 V. Each source is located at the center of the edge of the wedge part (see Fig. 1). Using CST software, in Fig. 5(a) we give the distribution of the amplitude of electric fields ($|E_z|$) near the surface of the sample with $R = 0\ \Omega$ at 1.56 GHz corresponding to $\mu_x = 0.02$ in the rectangular part. $|E_z|$ is in units of V/m. The wave is strongly reflected by the MNZ medium. In the experiments, we directly measure the voltage magnitude between the crossing node of the microstrip lines and the ground plane, which is the integral value of $|E_z|$ in the z direction. After signals are input to the samples, using a differential probe (Agilent P7260) and an oscilloscope (TektronixTDS7704B), we measure the voltage signals at all nodes, one by one. Since the signal is time harmonic, we record the peak-to-peak value from the oscilloscope, which is twice the voltage amplitude. By analyzing the recorded peak-to-peak values at all nodes, we obtain the distribution of the voltage amplitude. Figure 5(b) gives the measured distribution of the voltage amplitude (denoted by U in units of mV) in a sample with $R = 0\ \Omega$ at 1.56 GHz. Strong reflection also occurs at the entrance face of the MNZ medium. Figures 6 and 7 show the cases of samples with $R = 100$ and 1000 Ω, respectively. Comparing Fig. 6 with Fig. 5, we see that the fields are enhanced and collimated in the MNZ medium. Note that the collimation is not due to the bending of the microstrip lines in the rectangular part. In fact, when the rectangular part does not have lumped elements, a wave will go into the rectangular part with the

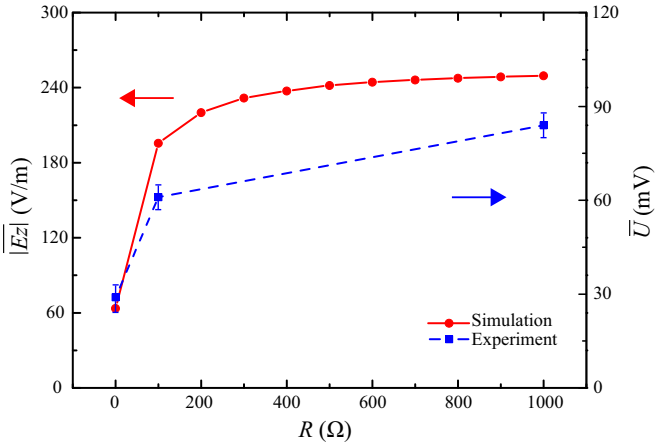

FIG. 8. (Color online) The simulated average values of $|E_z|$ (solid circles) along the x direction in the middle microstrip line of the rectangular part when R changes from 0 to 1000 Ω with a step of 100 Ω at 1.56 GHz. The measured average values of U in the same region for $R = 0$, 100, and 1000 Ω at 1.56 GHz are shown by the solid squares.

same direction in the wedge part (this figure is not shown). Comparing Fig. 7 with Fig. 6, we see that the collimated fields are further enhanced because the imaginary part of k_x decreases. Finally, in Fig. 8 we perform the average of $|E_z|$ and U. The solid circles give the simulated average values of $|E_z|$ along the x direction in the middle microstrip line of the rectangular part when R changes from 0 to 1000 Ω with a step of 100 Ω at 1.56 GHz. The measured average values of U in the same region for $R = 0$, 100, and 1000 Ω at 1.56 GHz are shown by the solid squares. With an increase of R, the fields in the MNZ medium are boosted.

IV. CONCLUSION

In conclusion, loss-induced abnormal propagations including collimation and field enhancement are observed in MNZ media based on 2D TLs with engineered dissipation. Our experimental results not only extend the knowledge of wave propagations connected with losses, but also reveal the loss-induced topological transition of dispersion at a fixed frequency.

ACKNOWLEDGMENTS

The authors thank X. H. Xu, Y. Y. Hu, and L. He for help with the experiments. This work was funded by the National Basic Research Program of China (Grant No. 2011CB922001), the National Natural Science Foundation of China (Grants No. 11234010 and No. 11204217), Innovation Program of Shanghai Municipal Education Commission (Grant No. 14ZZ040), and the Fundamental Research Funds for the Central Universities.

[1] R. A. Shelby, D. R. Smith, and S. Schultz, Science **292**, 77 (2001).
[2] R. W. Ziolkowski, Phys. Rev. E **70**, 046608 (2004).
[3] N. Engheta, Science **340**, 286 (2013).
[4] S. Enoch, G. Tayeb, P. Sabouroux, N. Guérin, and P. Vincent, Phys. Rev. Lett. **89**, 213902 (2002).
[5] Q. Cheng, W. X. Jiang, and T. J. Cui, Phys. Rev. Lett. **108**, 213903 (2012).
[6] M. Silveirinha and N. Engheta, Phys. Rev. Lett. **97**, 157403 (2006).
[7] R. P. Liu, Q. Cheng, T. Hand, J. J. Mock, T. J. Cui, S. A. Cummer, and D. R. Smith, Phys. Rev. Lett. **100**, 023903 (2008).
[8] V. C. Nguyen, L. Chen, and K. Halterman, Phys. Rev. Lett. **105**, 233908 (2010).
[9] X. Q. Huang, Y. Lai, Z. H. Hang, H. H. Zheng, and C. T. Chan, Nat. Mater. **10**, 582 (2011).
[10] A. A. Basharin, C. Mavidis, M. Kafesaki, E. N. Economou, and C. M. Soukoulis, Phys. Rev. B **87**, 155130 (2013).
[11] K. Halterman and S. M. Feng, Phys. Rev. A **78**, 021805 (2008).
[12] J. Luo, W. X. Lu, Z. H. Hang, H. Y. Chen, B. Hou, Y. Lai, and C. T. Chan, Phys. Rev. Lett. **112**, 073903 (2014).
[13] A. Ciattoni, C. Rizza, and E. Palange, Phys. Rev. A **81**, 043839 (2010).
[14] H. Suchowski, K. O'Brien, Z. J. Wong, A. Salandrino, X. B. Yin, and X. Zhang, Science **342**, 1223 (2013).
[15] A. R. Davoyan, A. M. Mahmoud, and N. Engheta, Opt. Express **21**, 3279 (2013).
[16] S. M. Feng, Phys. Rev. Lett. **108**, 193904 (2012).
[17] L. Sun, S. M. Feng, and X. D. Yang, Appl. Phys. Lett. **101**, 241101 (2012).
[18] J. Gao, L. Sun, H. X. Deng, C. J. Mathai, S. Gangopadhyay, and X. D. Yang, Appl. Phys. Lett. **103**, 051111 (2013).
[19] G. V. Eleftheriades, A. K. Iyer, and P. C. Kremer, IEEE Trans. Microwave Theory Technol. **50**, 2702 (2002).
[20] J. S. Hong and M. J. Lancaster, *Microstrip Filters for RF/Microwave Application* (Wiley, New York, 2001).
[21] Y. J. Feng, X. H. Teng, J. M. Zhao, Y. Chen, and T. Jiang, J. Appl. Phys. **100**, 114901 (2006).
[22] A. V. Chshelokova, P. V. Kapitanova, A. N. Poddubny, D. S. Filonov, A. P. Slobozhanyuk, Y. S. Kivshar, and P. A. Belov, J. Appl. Phys. **112**, 073116 (2012).
[23] H. N. S. Krishnamoorthy, Z. Jacob, E. Narimanov, I. Kretzschmar, and V. M. Menon, Science **336**, 205 (2012).